


Stability and superfluidity of the Bose-Einstein condensate in a two-leg ladder with magnetic field

Yue Jian,^{1,2} Xin Qiao,¹ Jun-Cheng Liang,¹ Zi-Fa Yu,¹ Ai-Xia Zhang,¹ and Ju-Kui Xue^{1,*}
¹*College of Physics and Electronic Engineering, Northwest Normal University, Lanzhou 730070, China*
²*Department of Basic Sciences, Lanzhou Institute of Technology, Lanzhou 730050, China*

 (Received 23 March 2021; accepted 27 July 2021; published 13 August 2021)

The stability and superfluidity of the Bose-Einstein condensate in two-leg ladder with magnetic field are studied. The dispersion relation and the phase diagram of the system are obtained. Three phases are revealed: the Meissner phase, the biased ladder (BL) phase, and the vortex phase. The dispersion relation and phase transition of the system strongly depend on the magnitude of atomic interaction strength, the rung-to-leg coupling ratio and the magnetic flux. Particularly, the change of the energy band structure in the phase transition region is modified significantly by the atomic interaction strength. Furthermore, based on the Bogoliubov theory, the energetic and dynamical stability of the system are investigated. The stability phase diagram in the full parameter space is presented, and the dependence of superfluidity on the dispersion relation is illustrated explicitly. The atomic interaction strength can produce dynamical instability in the energetic unstable region and can expand the superfluid region. The results show that the stability of the system can be controlled by the atomic interaction strength, the rung-to-leg coupling ratio and the magnetic flux. In addition, the excitation spectrums in the Meissner phase, BL phase and vortex phase are further studied. The modulation of the excitation spectrum and the energetic stability of the system by the atomic interaction strength, the rung-to-leg coupling ratio and magnetic flux is discussed. Finally, through the numerical simulation, the dynamical instability of the system is verified by the time evolution of the Bloch wave and rung current. This provides a theoretical basis for controlling the superfluidity of the system.

DOI: [10.1103/PhysRevE.104.024212](https://doi.org/10.1103/PhysRevE.104.024212)

I. INTRODUCTION

Ultracold bosonic atoms in optical lattices offer a clean and highly controlled experimental platform to explore intriguing phenomena in condensed physics. By overlapping and interfering laser beams, various kinds of trapping potentials can be created and the atomic interaction strength can also be controlled by magnetic fields or by selecting different atomic species [1–5]. The realization of optical lattice has stimulated a lot of theoretical and experimental research work and found some interesting phenomena [6–10]. In particular, recent progress in creating artificial gauge fields for ultracold atoms in discrete as well as continuum systems has opened up many new fields for the study of quantum phase transitions, such as vortex nucleation [11,12], the Hofstadter model [13,14], and vortices [15,16]. The behavior of charged particles in magnetic field can be simulated by Bose-Einstein condensate (BEC) in an optical lattice subject to an artificial magnetic field. The atoms can be manipulated by the laser-assisted tunneling to induce a phase resembling an effective magnetic field, i.e., the so-called artificial magnetic field [17,18]. The introduction of artificial magnetic field induces a Lorentz like force and breaks time-reversal symmetry and modifies the energy band structure of the system. The realization of the artificial magnetic field in an optical lattice has provided physicists a new fertile ground for exploring

many aspects of nonlinear phenomena, including quantum hall states [19,20], the Bose glass phase [21], and the Bose-Hubbard model [22,23].

The bosonic two-leg ladder is the simplest model for studying the response of bosons to a magnetic field. Due to the experimental observations are particularly easy to interpret, researchers show great interests in this system both theoretically and experimentally [24–26]. Thus, the ladder system opens up a significant controllable path to study the Hofstadter butterfly [27,28], the Mott-insulator-superfluid phases [29] and the topologically protected phases [30]. Recently, the ladder system has been used to successfully realize the phase transition from Meissner to vortex state with noninteracting impact [31], which not only lays the foundation for the cold atom system to simulate the superconductor but also provides a new way to realize the spin-orbit coupling in low-dimensional quantum gases. For the interacting case, the interplay between single-particle degeneracies and atomic interaction leads to interesting physics, such as Mott phases with staggered loop currents [32], vortex flux, charge density waves, and biased ladder phase [33,34]. However, most of the studies about the two-leg ladder system focus on the discussion of the ground state and the phase transition process, but the stability of the system, especially its superfluidity, is still not clear [35–37]. Furthermore, how the atomic interaction strength modifies the dispersion relation and the ground-state phase diagram of the system is still an open subject.

In the optical lattice, superfluidity of BEC can be represented by a Bloch wave, which can be regarded as a plane

*xuejk@nwnu.edu.cn

wave modulated by the periodic potential [38]. Bloch wave and Bloch band play important role to the study of superfluidity and many of its related phenomena in this periodic system. The Landau instability is determined by whether the elementary excitation around a Bloch wave lowers the system's energy. If it does not, then the Bloch wave is a local energy minimum of the system which represents a superfluidity, the system is energetic stable. Otherwise, the Bloch wave is an energy saddle point which results in Landau instability, i.e., energetic unstable [39]. Apart from the atomic interaction, the BEC in the optical lattice is always dynamical stable. Dynamical unstable occurs when both the atomic interaction and the periodic lattice exist, which causes the system to deviate from the original Bloch state during small transient disturbance [40].

In this work, we study the stability and superfluidity of BEC with atomic interaction trapped in two-leg ladder subject to an artificial magnetic field. By calculating the ground-state energy, atomic density, and the rung current, the dispersion relation and the ground-state phase diagram are obtained. Three phases in the ground state are revealed: the Meissner phase, the biased ladder (BL) phase, and the vortex phase. The atomic interaction strength, the rung-to-leg coupling ratio, and the magnetic flux can modify the dispersion relation and result in the phase transition. Furthermore, the energetic and dynamical instability of the system are studied based on the Bogoliubov theory. The stability phase diagram in the full parameter space is obtained, the physical mechanism of superfluid generation is further clarified. The excitation spectrums in the Meissner phase, BL phase, and vortex phase are also studied respectively. The modulation of the excitation spectrum and the energetic stability of the system by the atomic interaction strength, the rung-to-leg coupling ratio and magnetic flux is discussed. Finally, through the numerical simulation, the dynamical instability is verified by the time evolution of the Bloch wave and rung current.

This paper is organized as follows. In Sec. II, we present the model of BEC trapped into a two-leg ladder with an artificial magnetic field. In Sec. III, the dispersion relation and the ground-state phase diagram are presented in detail. In Sec. IV, the energetic and dynamical instability are studied based on the Bogoliubov theory. The stability phase diagram and the physical mechanism of superfluid generation are given. In Sec. V, the excitation spectrums in the three phases are determined. In Sec. VI, the numerical validation results of the dynamical stability are clearly presented. Finally, in Sec. VII, a brief summary is given.

II. MODEL

We study the stability and superfluidity of BEC in two-leg ladder subject to an artificial magnetic field. The two-leg bosonic ladder is an infinite ladder composed of square plaquettes. In the experiment [31], along the rungs, by using a superlattice, an array of isolated double-well potentials is generated, and there is a bare tunneling J_x and an energy offset Δ that inhibits left-right tunneling inside each ladder. The pair of running-wave beams with frequency difference $\omega = \omega_1 - \omega_2 = \Delta/\hbar$ can create an artificial magnetic field, which restores the tunneling and induces a complex hopping

term $\tilde{K} \simeq J_x V_K^0 / (2\sqrt{2}\Delta)$ and has a spatially dependent phase, where V_K^0 is the running-wave beams intensity. The tunneling along the legs is determined through $\tilde{J} = J_y \mathcal{J}_0[V_K^0 / (2\sqrt{2}\Delta)]$, where J_y is tunneling along the legs and \mathcal{J}_0 is Bessel function of order 0. The total phase accumulated by a particle when completing a closed trajectory on a single plaquette corresponds to the magnetic flux per unit cell. By changing the wavelength of the running-wave beams or the angle between them, one can in principle engineer any flux. The tight-binding Hamiltonian for this two-leg bosonic ladder is given by

$$\begin{aligned} \hat{H} = & -\tilde{J} \sum_n (e^{i\phi} \hat{a}_{n,L} \hat{a}_{n+1,L}^\dagger + e^{-i\phi} \hat{a}_{n,R} \hat{a}_{n+1,R}^\dagger + \text{H.c.}) \\ & -\tilde{K} \sum_n (\hat{a}_{n,L}^\dagger \hat{a}_{n,R} + \text{H.c.}) \\ & + \frac{\tilde{g}}{2} \sum_n (\hat{a}_{n,L}^\dagger \hat{a}_{n,L} \hat{a}_{n,L} \hat{a}_{n,L} + \hat{a}_{n,R}^\dagger \hat{a}_{n,R} \hat{a}_{n,R} \hat{a}_{n,R}), \end{aligned} \quad (1)$$

where the summation index and subscript n refer to the n th site, $\hat{a}_{n,\sigma}$ and $\hat{a}_{n,\sigma}^\dagger$ are the bosonic annihilation and creation operators on the left or right leg of the ladder at position n (σ stands for L or R). \tilde{J} and \tilde{K} represent the hopping matrix elements along the legs and rungs of the ladder, respectively, and ϕ is the magnetic flux piercing each unit cell; \tilde{g} is atomic interaction strength between arbitrary two atoms in a site; H.c. denotes the conjugate term.

Using the mean-field approximation, i.e., $\langle \hat{a}_{n,\sigma} \rangle = a_{n,\sigma}$, the tight-binding Hamiltonian (1) is given by

$$\begin{aligned} H = & -\tilde{J} \sum_n (e^{i\phi} a_{n,L} a_{n+1,L}^* + e^{-i\phi} a_{n,R} a_{n+1,R}^* + \text{H.c.}) \\ & -\tilde{K} \sum_n (a_{n,L}^* a_{n,R} + \text{H.c.}) + \frac{\tilde{g}}{2} \sum_n (|a_{n,L}|^4 + |a_{n,R}|^4), \end{aligned} \quad (2)$$

where the $a_{n,\sigma}$ is the probability amplitude of atoms on the leg of the ladder at position n . In order to study the dynamic characteristics of the system, by using the Heisenberg equation of motion ($i\hbar da_{n,\sigma}/dt = \partial H/\partial a_{n,\sigma}^*$), the discrete nonlinear Schrödinger equation associated with $a_{n,\sigma}$ corresponding to Hamiltonian (2) can be obtained,

$$\begin{aligned} i\dot{a}_{n,L} = & -(e^{-i\phi} a_{n+1,L} + e^{i\phi} a_{n-1,L}) - K a_{n,R} + g |a_{n,L}|^2 a_{n,L} \\ i\dot{a}_{n,R} = & -(e^{i\phi} a_{n+1,R} + e^{-i\phi} a_{n-1,R}) - K a_{n,L} + g |a_{n,R}|^2 a_{n,R}, \end{aligned} \quad (3)$$

where we used the natural element $\hbar = 1$, $K = \tilde{K}/\tilde{J}$, and $g = \tilde{g}/\tilde{J}$, and $a_{n,\sigma}$ satisfies the normalization condition, i.e., $\sum_n (|a_{n,L}|^2 + |a_{n,R}|^2) = 1$. Note that the time has been rescaled as $t \rightarrow [\hbar/\tilde{J}]t$.

It is easy to measure the currents in real space along the legs and rungs of ladder in experiment, so we can define current operators along the legs and rungs as

$$\begin{aligned} j_{n,\sigma}^\parallel = & i(e^{\pm i\phi} a_{n+1,\sigma}^\dagger a_{n,\sigma} - \text{H.c.}) \\ j_n = & iK(a_{n,R}^\dagger a_{n,L} - \text{H.c.}). \end{aligned} \quad (4)$$

In addition, the chiral current j_c along the legs plays an important role in characterizing each phase. The chiral current j_c is

defined as

$$j_c = j_{n,L}^{\parallel} - j_{n,R}^{\parallel}. \quad (5)$$

III. THE DISPERSION RELATION AND PHASE DIAGRAM

We employ the two superimposed Bloch waves (the superposition state)

$$a_{n,\sigma} = a_{\sigma+} e^{i(kn-\mu t)} + a_{\sigma-} e^{-i(kn+\mu t)} \quad (6)$$

as the stationary solution of Eq. (3), so that

$$\begin{aligned} \mu a_{L\pm} &= -2a_{L\pm} \cos(k \mp \phi) - K a_{R\pm} + g|a_{L\pm}|^2 a_{L\pm} \\ &\quad + 2g|a_{L\mp}|^2 a_{L\pm} \\ \mu a_{R\pm} &= -2a_{R\pm} \cos(k \pm \phi) - K a_{L\pm} + g|a_{R\pm}|^2 a_{R\pm} \\ &\quad + 2g|a_{R\mp}|^2 a_{R\pm}, \end{aligned} \quad (7)$$

where k and μ are the quasimomentum and chemical potential of the system.

For noninteracting particles, the dispersion relation of the band is described as follows:

$$\mu_{\pm} = -2 \cos k \cos \phi \pm \sqrt{K^2 + 4 \sin^2 k \sin^2 \phi}. \quad (8)$$

Because the characteristics of the lower band are very important for study the ground state and phase transition of the system, we mainly discuss the dispersion relationship of the lower band. It is obvious that the period of the two bands is 2π . Consistent with relevant theoretical and experimental researches, as the rung-to-leg coupling ratio K increases, the lower band minimum shifts from two nonzero k values to $k = 0$, and the two nonzero k are degenerate and symmetric around the origin. Using $\partial \mu_- / \partial k = 0$, we obtain the critical condition for this bifurcation. For $K \geq 2 \sin \phi \tan \phi$, the lower band μ_- has a single minimum at $k = 0$, while for $K < 2 \sin \phi \tan \phi$, μ_- has two minima at $k = \pm k_0$, where $k_0 = \arccos \sqrt{K/4 \tan^2 \phi + \cos^2 \phi}$. The ground states of these two lower band structures correspond to the Meissner phase and the vortex phase, respectively.

Now we concentrate on the weakly atomic interacting limit and calculate how the phase transition is affected by the presence of atomic interaction. The dispersion relation Eq. (7) depends on the magnitude of atomic interaction strength, the rung-to-leg coupling ratio and the magnetic flux, thus it cannot be obtained analytically, but can be described numerically. By calculating the ground-state atomic density and the rung current, we find three phases which are shown in Fig. 1: (1) The Meissner phase corresponds to the ground state of the zero quasimomentum state, where the atomic density is uniform, and equal and opposite currents flow along the two legs of the ladder. The rung current vanishes. (2) The BL phase, where the atomic density is uniform but different on the left and right legs. The fluid velocity is higher (lower) on the lower (higher) density leg, so the rung current is zero. (3) The vortex phase, where the atomic density is modulated along the ladder and has the rung current. Both the BL phase and the vortex phase corresponds to the ground state of the nonzero quasimomentum state and these phases have a twofold degeneracy which are associated with symmetry $k_0 \rightarrow -k_0$, the choice of the leg with a higher (lower) density is arbitrary. In the BL

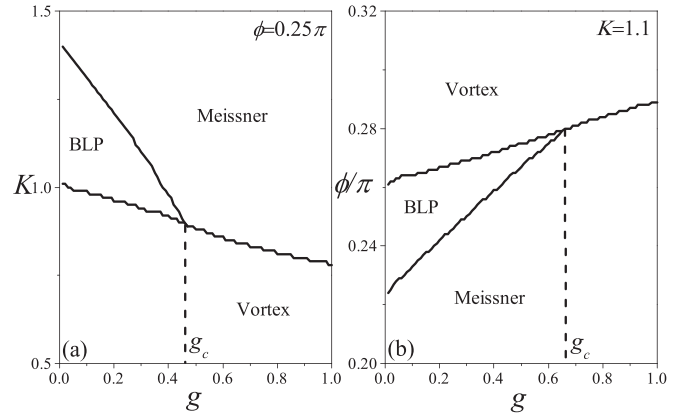


FIG. 1. The ground-state phase diagrams in K - g plane for $\phi = \pi/4$ (a) and in ϕ - g plane for $K = 1.1$ (b).

phase, due to only one of the two minima is macroscopically populated, the system in this phase can be described by the plane-wave state, i.e., $a_{\sigma-} = 0$ in Eq. (6), which is consistent with the system in Meissner phase. Furthermore, the vortex phase is characterized by a macroscopic occupation of a superposition state involving two momentum modes $k = \pm k_0$, so the system in vortex phase can be described by the superposition state.

The ground-state phase diagram in K - g plane for $\phi = \pi/4$ is depicted in Fig. 1(a). It can be clearly seen that there exists a tricriticality g_c at the phase boundary of the Meissner, BL and vortex phases. With K increases, when $g < g_c$, the system experiences vortex-BL-Meissner phase transition, while when $g > g_c$, the system experiences vortex-Meissner phase transition. Figure 1(b) shows the ground-state phase diagram in ϕ - g plane for $K = 1.1$. Similarly to Fig. 1(a), there also exists a tricriticality g_c at the phase boundary of the three phases. With ϕ increases, when $g < g_c$, the system experiences Meissner-BL-vortex phase transition, while when $g > g_c$, the system experiences Meissner-vortex phase transition. According to the two phase diagrams, with the increase of g , the BL phase region decreases until it disappears when $g = g_c$, while the Meissner phase region increases. This indicates that the stronger atomic interaction strength makes the ground state of the system easier to be in the Meissner phase, but difficult to maintain the BL phase. That is, when $g < g_c$, although the particle number density distribution is uneven on the left and right legs, the particles only propagate on the left and right legs without mutual interference within a certain parameter range. In addition, the magnetic flux ϕ also plays an important role for the phase transition of the system. The system is more likely to be in the vortex phase under a larger ϕ , and when $\phi \rightarrow \frac{\pi}{2}$, the system is only in the vortex phase. Since the BL phase region under the K - g plane is much larger than that under the ϕ - g plane, the phase transition is sensitive to the intensity of ϕ . In short, the phase transition of the system depends on the magnitude of the atomic interaction strength, the rung-to-leg coupling ratio and the magnetic flux.

Figure 2 shows the dispersion relations under different phases with the smaller atomic interaction strength ($g = 0.2 < g_c$) and the larger atomic interaction strength ($g = 0.8 > g_c$). Corresponding to Fig. 1, when $g = 0.2 < g_c$, the

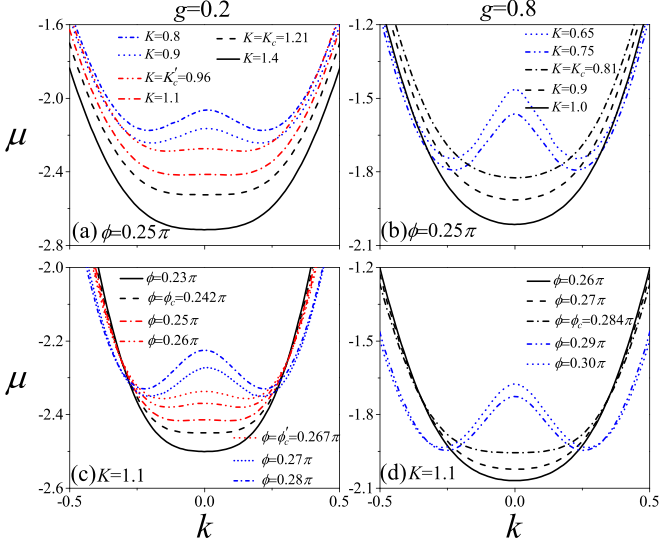


FIG. 2. The dispersion relations of the lower band under $g = 0.2 < g_c$ and $g = 0.8 > g_c$. The black line, red line, and blue line indicate that the ground state of the system is in the Meissner phase, the BL phase, and the vortex phase, respectively.

ground state shows three phases and Figs. 2(a) and 2(c), respectively, draw the dispersion relations under the three different phases. The lower band has two structures in the parameter space: In the Meissner phase, the lower band minimum is at $k = 0$, the system is in the zero quasimomentum state; while in the BL or vortex phase, the lower band minimum is at the two symmetric quasimomentum $\pm k_0$, the system is in the nonzero quasimomentum state. In addition, due to the emergence of the BL phase in the transition region of zero quasimomentum state to nonzero quasimomentum state, the lower energy band structure gradually transition from the zero quasimomentum state to nonzero quasimomentum state with K (ϕ) decrease (increase).

When $g = 0.8 > g_c$, the ground state of the system only shows the Meissner phase and the vortex phase, Figs. 2(b) and 2(d), respectively, draw the dispersion relations under the two different phases. As shown in the figures, the lower band still has two structures, that is, under the Meissner phase, the magnetic ladder system is in the zero quasimomentum state, and under the vortex phase, the system is in the nonzero quasimomentum state. However, due to the absence of the BL phase, the lower energy band changes abruptly at the phase transition point.

In order to further study the phase transition, the chiral current j_c and quasimomentum $|k_0|$ corresponding to the ground state as functions of K and ϕ for $g = 0$, $g = 0.2$ and $g = 0.8$ are plotted in Fig. 3. As shown in Fig. 3(a), for fixed ϕ , j_c increases with the increase of K in the vortex and BL phases, and j_c reaches saturation in the Meissner phase. Figure 3(b) shows that, for fixed K , in the Meissner phase, j_c increases with the increase of ϕ , while in the BL and vortex phases, j_c decreases with the increase of ϕ . When $g = 0$, the system experiences vortex-Meissner phase transition with K increases or ϕ decreases, during which j_c is continuous across the phase transition point. However, atomic interaction breaks this continuity. j_c has a discontinuous jump between the vortex phase

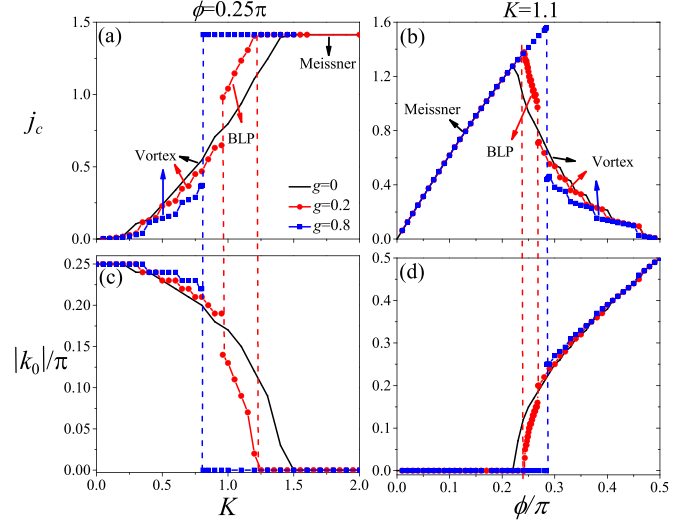


FIG. 3. [(a) and (b)] The chiral current j_c as a function of K and ϕ . [(c) and (d)] The quasimomentum $|k_0|$ corresponding to the ground state as a function of K and ϕ . The dotted line represents the dividing line of the different phases.

and BL phase at $g = 0.2$ or the vortex phase and Meissner phase at $g = 0.8$. Especially, since absence of BL phase at $g = 0.8$, j_c has strong jump across the phase transition point. In addition, it can be clearly seen from Figs. 3(c) and 3(d) that the system belongs to the nonzero quasimomentum state ($|k_0| \neq 0$) in the vortex phase or BL phase and the zero quasimomentum state ($|k_0| = 0$) in the Meissner phase. Moreover, the continuity of $|k_0|$ against K and ϕ is consistent with that of j_c against K and ϕ .

In general, atomic interaction causes j_c or $|k_0|$ has a discontinuous jump between the vortex and BL phases or vortex and Meissner phases and makes the ground state of the system easier to be in the Meissner phase. This discontinuity represents a first-order transition, which is caused by the transition from the vortex phase to BL phase or Meissner phase. That is, the atomic density changes from a modulated form in the vortex phase to an uniform form in the BL phase or Meissner phase along the ladder. Especially in the case of $g = 0.8 > g_c$, due to the absence of BL phase, the lower band structure changes from double-well structure to single-well structure rapidly, resulting in a strong jump of j_c or $|k_0|$ at the phase transition point. However, when the BL phase exists, j_c or $|k_0|$ is continuous while its slope with K or ϕ is discontinuous across the phase transition point between the BL and Meissner phase, indicating the transition from BL phase to Meissner phase is a second-order transition. With the increase of K or the decrease of ϕ , the atomic density difference between the left and right legs in BL phase gradually decreases until it tends to 0 in the Meissner phase. This is a continuous changing process, so the transition of the lower band structure from the nonzero quasimomentum state to zero quasimomentum state is gradually, and j_c or $|k_0|$ is continuous with K or ϕ .

In the experiment [31], a local density measurement can distinguish the three phases. For the Meissner phase, the chiral current is saturated; for the vortex phase, the spatial inhomogeneities of the chiral current along each leg is consistent with

the transition to vortex phase. For the BL phase, atoms appear to have a state which is translationally invariant along the ladder, and has a nonsaturated chiral current. Another direct probe of these states is the time-of-flight measurement. In the Meissner phase, there is only one momentum peak for each leg, the momentum peaks are located at $k = \pm\pi/(4d_y)$, where d_y is lattice constants along the legs; in the BL phase, there is still only one momentum peak for each leg, but the characteristic momentum is reduced to $k < \pm\pi/(4d_y)$. In the vortex phase, there are two different momenta on each leg and the momentum distribution is bimodal [41]. In addition, the BL phase can be readily identified by the susceptibility measurement [33].

IV. THE ENERGETIC AND DYNAMICAL INSTABILITY

We now study the stability of BEC in two-leg ladder by using the Bogoliubov theory. The stability analysis of such a

state can be carried out by perturbing the superimposed Bloch waves with small-amplitude phonons:

$$a_{n,\sigma} = [a_{\sigma+} + u_{\sigma+}e^{i(qn-i\omega t)} + v_{\sigma+}^*e^{-(iqn-i\omega t)}]e^{i(kn-\mu t)} + [a_{\sigma-} + u_{\sigma-}e^{i(qn-i\omega t)} + v_{\sigma-}^*e^{-(iqn-i\omega t)}]e^{-i(kn+\mu t)}, \quad (9)$$

where $u_{\sigma\pm}$, $v_{\sigma\pm}^*$, q , and ω are the two quasiparticle amplitudes, the quasimomentum, and the frequency of the perturbation, respectively. The perturbation is a periodic disturbance that depends on the quasimomentum excited by the particle and the position of the optical lattice. Experimentally, this perturbation can be produced by a sudden movement of the magnetic potential along the lattice. Substituting Eq. (9) into Eq. (3) and retaining only linear terms in the perturbation, we obtain Bogoliubovde Gennes (BDG) equation $\hat{A}\psi = \omega\psi$ with $\psi = (u_{L+}, u_{L-}, u_{R+}, u_{R-}, v_{L+}, v_{L-}, v_{R+}, v_{R-})^T$, where

$$\hat{A} = \begin{bmatrix} U(a+q) & 2ga_{L+}a_{L-}^* & -K & 0 & ga_{L+}^2 & 2ga_{L+}a_{L-} & 0 & 0 \\ 2ga_{L+}^*a_{L-} & U(b-q) & 0 & -K & 2ga_{L+}a_{L-} & ga_{L-}^2 & 0 & 0 \\ -K & 0 & V(b+q) & 2ga_{R+}a_{R-}^* & 0 & 0 & ga_{R+}^2 & 2ga_{R+}a_{R-} \\ 0 & -K & 2ga_{R+}^*a_{R-} & V(a-q) & 0 & 0 & 2ga_{R+}a_{R-} & ga_{R-}^2 \\ -ga_{L+}^* & -2ga_{L+}^*a_{L-}^* & 0 & 0 & -U(a-q) & -2ga_{L+}^*a_{L-} & K & 0 \\ -2ga_{L+}^*a_{L-}^* & -ga_{L-}^* & 0 & 0 & -2ga_{L+}a_{L-}^* & -V(b+q) & 0 & K \\ 0 & 0 & -ga_{R+}^* & -2ga_{R+}^*a_{R-}^* & K & 0 & -V(b-q) & -2ga_{R+}^*a_{R-} \\ 0 & 0 & -2ga_{R+}^*a_{R-}^* & -ga_{R-}^* & 0 & K & -2ga_{R+}a_{R-}^* & -V(a+q) \end{bmatrix} \quad (10)$$

with $U(a \pm q) = -2 \cos(k - \phi \pm q) + 2g|a_{L+}|^2 + 2g|a_{L-}|^2 - \mu$, $U(b \pm q) = -2 \cos(k + \phi \pm q) + 2g|a_{L+}|^2 + 2g|a_{L-}|^2 - \mu$, $V(a \pm q) = -2 \cos(k - \phi \pm q) + 2g|a_{R+}|^2 + 2g|a_{R-}|^2 - \mu$, $V(b \pm q) = -2 \cos(k + \phi \pm q) + 2g|a_{R+}|^2 + 2g|a_{R-}|^2 - \mu$. As discussed before, the system in the Meissner and BL phases can be well described by the plane-wave state, so both the energetic and dynamical stability in Meissner and BL phases are actually described with the Bloch wave quasiparticle excitation, i.e., $a_{n,\sigma} = [a_{\sigma+} + u_{\sigma+}e^{i(qn-i\omega t)} + v_{\sigma+}^*e^{-(iqn-i\omega t)}]e^{i(kn-\mu t)}$ ($a_{\sigma-} = u_{\sigma-} = v_{\sigma-}^* = 0$). Therefore, \hat{A} is reduced to a fourth-order matrix.

The dynamical instability is excited if \hat{A} has one or more nonzero imaginary eigenvalues. In this case, the instability is characterized by the exponential growth of the perturbation. The system is dynamical stable if all eigenvalues are real numbers. Furthermore, the Landau instability, i.e., energetic instability, can be studied by solving the BDG equation, $\beta\psi = \hat{\tau}_z \hat{A}\psi$, where $\hat{\tau}_z = \begin{pmatrix} I & 0 \\ 0 & -I \end{pmatrix}$ and I is the identity matrix. The system is said to be Landau unstable if one or more eigenvalues of $\hat{\tau}_z \hat{A}$ are negative. Physically, the Bloch wave with Landau instability is not the local energy minimum of the system. The system is energetic stable if all eigenvalues are positive; at this time the Bloch wave has the local minimum energy which represents the existence of superfluid.

We systematically study the stability of the system at the lower band for various parameters. The stability phase diagram in q - k plane for different K and g is clearly depicted

in Fig. 4. Due to the symmetry in q - k plane, we only show the region of $0 \leq k \leq \pi$ and $0 \leq q \leq \pi$. As K (for fixed g) or g (for fixed K) increases, the superfluid region gradually shifts from around $k \neq 0$ region to around $k = 0$ region, which corresponds to the transition of the system from the nonzero quasimomentum state to the zero quasimomentum state. The superfluid region appears near the ground state, which is closely related to the quasimomentum k_0 corresponding to the lowest energy of the system, and strongly depends on K or g modified dispersion relations. The distribution of the superfluid region can clearly reflect the phase transition of the system, i.e., the system experiences the vortex-BL-Meissner or vortex-Meissner phase transition with K (for fixed g) or g (for fixed K) increases, which agrees with the results show in Fig. 1(a). In the case of $g = 0$, the superfluid region increases with the increase of K in the vortex phase until it becomes stable in the Meissner phase, which results from the K -modified dispersion relation. The system is always dynamical stable. However, in the case of $g \neq 0$, the atomic interaction can affect the stability of the system and produce dynamical instability in the energetic unstable region. With the increase of g , in the region away from k_0 , the dynamical unstable region increases, which indicates that the strong g cannot maintain the stability of the system in the region away from the ground state. In the vortex phase (the figures in Fig. 4 marked with inverted triangle symbol line), the stability of the system is described by the superposition state, the superfluid region

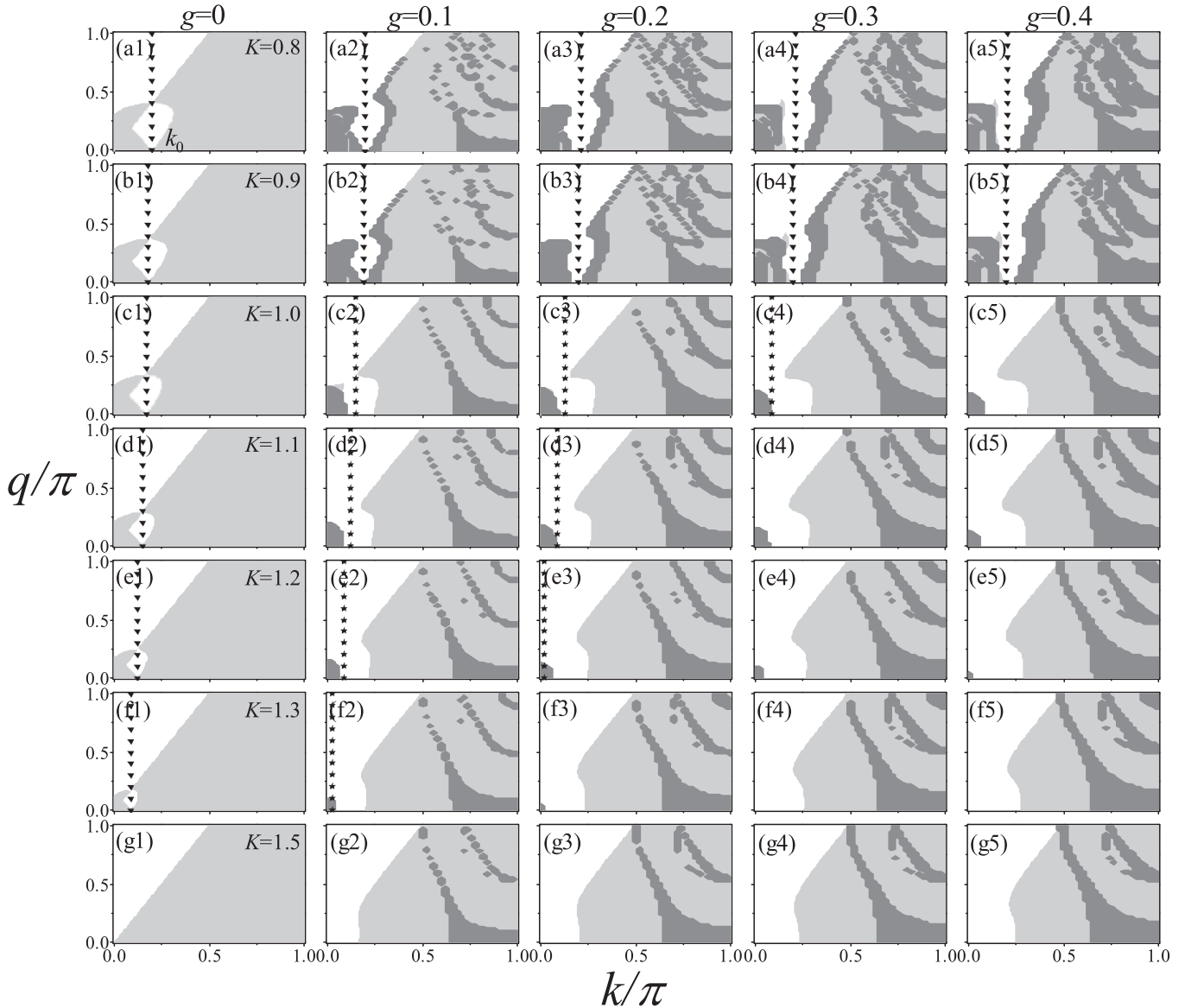


FIG. 4. The stability phase diagram in k - q plane for different K and g . $\phi = \pi/4$. From the first row to the seventh row: $K = 0.8, 0.9, 1.0, 1.1, 1.2, 1.3, 1.5$; from the first column to the fifth column: $g = 0, 0.1, 0.2, 0.3, 0.4$. Gray shaded region: the dynamical unstable region; light gray shaded region: the energetic unstable region; and white area: the stable superfluid region. The symbol line represents the quasimomentum $k = k_0$ corresponding to the ground state. The graphs with symbol line belong to nonzero quasimomentum state and the rest belong to zero quasimomentum state. The inverted triangle symbol indicates that the ground state is in the vortex phase, and the star symbol indicates that the ground state is in the BL phase.

decreases gradually with the increase of K for fixed g and almost does not change with the increase of g for fixed K . The boundary of the dynamical unstable region coincides with the boundary of the energetic unstable region near $k = k_0$, which clearly outlines the superfluid region of the system. In Meissner phase and BL phase, the stability of the system in all phase regions is actually revealed with the plane-wave state, the superfluid region expands with the increase of K (for fixed g) or g (for fixed K). In addition, during the transition from nonzero quasimomentum state to zero quasimomentum state, the superfluidity in the transition region is affected by the change of the energy band structure [Figs. 4(f2), (e3)–(f3), (d4)–(e4), and (c5)–(e5)]. That is, during the transition region,

the dynamical instability can occur near the ground state when the perturbation quasimomentum q is small.

Figure 5 shows the stability phase diagram in q - k plane for different ϕ and g . Similarly to Fig. 4, the superfluid region is always distributed around $k = k_0$, which strongly depends on ϕ or g modified dispersion relations. Distribution of the superfluid region corresponds to the ground-state phase diagram of the ϕ - g plane [Fig. 1(b)]. The system changes from zero quasimomentum state to nonzero quasimomentum state with the increase of ϕ , which makes the ground state experiences the Meissner-BL-vortex or Meissner-vortex phase transition. With the increase of ϕ , the dynamical unstable region increases, while the superfluid region decreases in the Meissner

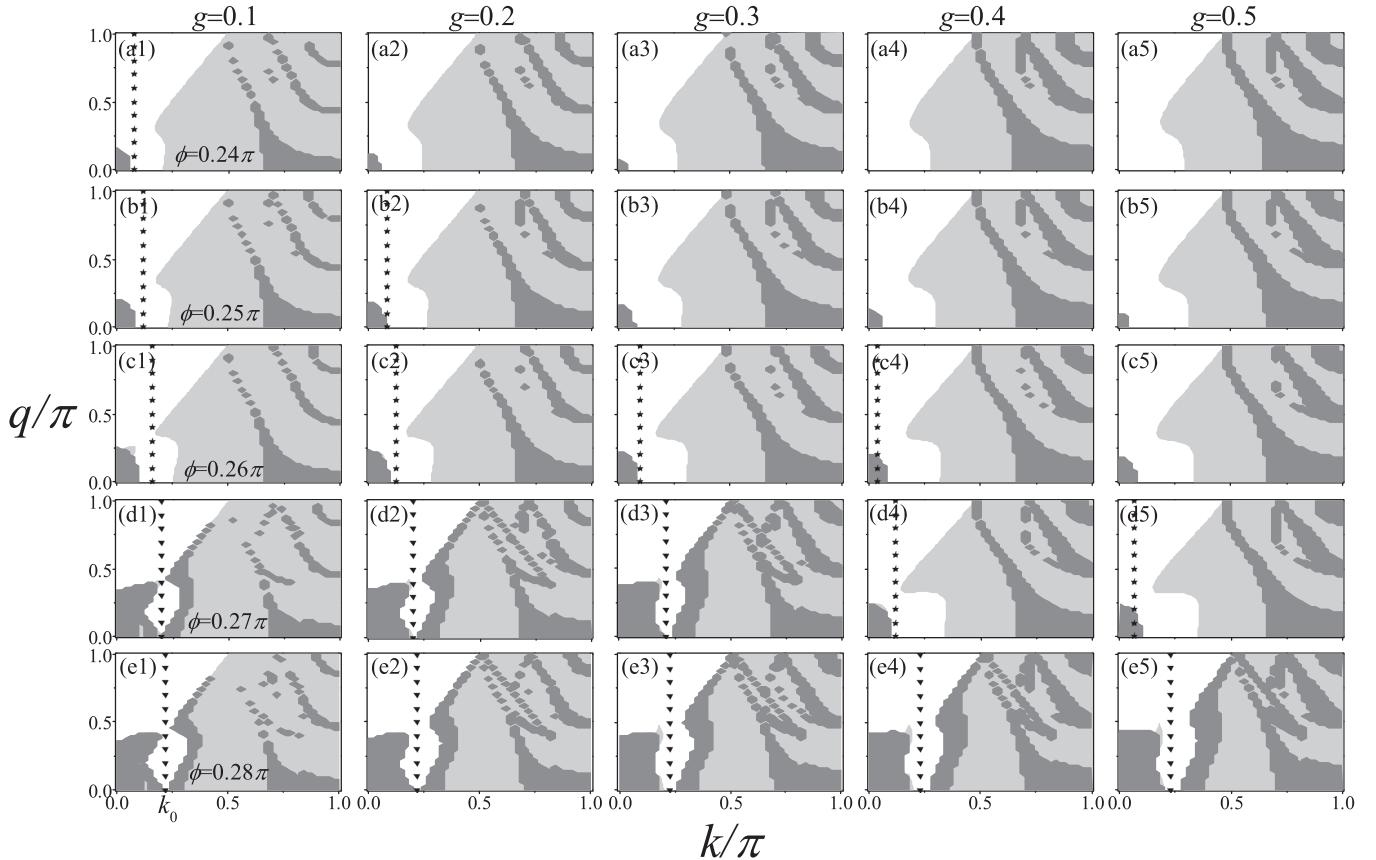


FIG. 5. The stability phase diagram in k - q plane for different ϕ and g . $K = 1.1$. From the first row to the fifth row: $\phi/\pi = 0.24, 0.25, 0.26, 0.27, 0.28$; from the first column to the fifth column: $g = 0.1, 0.2, 0.3, 0.4, 0.5$. Gray shaded region: the dynamical unstable region; light gray shaded region: the energetic unstable region; white area: the stable superfluid region. The symbol line represents the quasimomentum $k = k_0$ corresponding to the ground state. The graphs with symbol line belong to nonzero quasimomentum state and the rest belong to zero quasimomentum state. The inverted triangle symbol indicates that the ground state is in the vortex phase, and the star symbol indicates that the ground state is in the BL phase.

phase and BL phase and increases gradually in the vortex phase.

In order to further understand the dependence of stability on the K , ϕ and g , the stability phase diagrams and the corresponding quasimomentum of the ground state k_0 in different phase planes are depicted in Figs. 6. Figures 6(a) and 6(b) and Figs. 6(c) and 6(d) display the stability phase diagrams in K - k plane and ϕ - k plane, respectively. For $g = 0.2 < g_c$, according to the change of $|k_0|$ against K or ϕ (dashed lines), the ground state experiences the vortex-BL-Meissner phase transition as K (ϕ) increases (decreases). However, when $g = 0.8 > g_c$, $|k_0|$ mutates to zero abruptly as K (ϕ) increases (decreases) and only the vortex phase and the Meissner phase exist. The superfluid takes place around $k_0 \neq 0$ due to the nonzero quasimomentum state and around $k_0 = 0$ due to the zero quasimomentum state, which is closely related to the dispersion relations corrected by K and ϕ . Figures 6(e) and 6(f) demonstrate the stability phase diagram and the corresponding $|k_0|$ in the g - k plane; g can expand the superfluid region and make the system change from nonzero quasimomentum state to zero quasimomentum state, resulting in the superfluid region shifting from $k \neq 0$ to $k = 0$. This is also related to K and ϕ .

In a word, the energetic and dynamical instability of BEC in two-leg ladder with magnetic field can be precisely manipulated by the atomic interaction strength, the rung-to-leg coupling ratio and magnetic flux. The coupling effect of these parameters can make the superfluid appear in the region either around or deviated from the center of the Brillouin zone, which is closely related to quasimomentum of the ground state. The stability phase diagram can well illustrate the phase transition process of the system. Furthermore, the atomic interaction strength can expand the superfluid region and generate the dynamical instability in the region of energetic unstable. These can provide a theoretical evidence for control the superfluidity of the system in experiment.

V. EXCITATION SPECTRUM AND ENERGETIC STABILITY

Now let us discuss the excitation spectrum of the two-leg ladder system. The presence of the nonlinearity leads to rich phenomena within the collective excitation spectrum which are absent in the single-particle dispersion. The resulting spectral can be calculated by using the BDG equation to calculate the eigenvalue of \hat{A} given by Eq. (10).

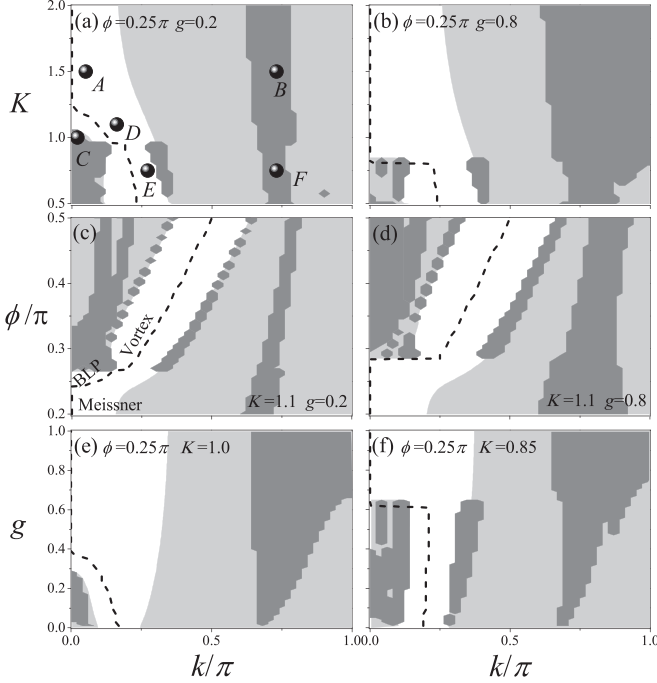


FIG. 6. The stability phase diagrams in K - k plane [(a) and (b)], ϕ - k plane [(c) and (d)], and g - k plane [(e) and (f)]. Gray shaded region: the dynamical unstable region; light gray shaded region: the energetic unstable region; and white area: the stable superfluid region. Dashed lines: the quasimomentum $|k_0|$ corresponding to the ground state. [(a) and (b)] $\phi = 0.25\pi$ and $q = 0.2\pi$; [(c) and (d)] $K = 1.1$ and $q = 0.25\pi$; [(e) and (f)] $\phi = 0.25\pi$ and $q = 0.2\pi$. Points A–F marked in Fig. 6(a) are selected for numerical simulation in different phase regions to verify the dynamical instability, and the relevant conclusions are shown in Figs. 9 and 10.

A. Excitation spectrum in the Meissner phase

In the Meissner phase, the ground-state solution for the condensate wave function is uniform and corresponds to a condensate occupying the $k = 0$ state, so that the system can be described by the plane-wave state. Then the matrix \hat{A} has the form

$$\hat{A} = \begin{bmatrix} U(-q) & -K & g\rho & 0 \\ -K & U(q) & 0 & g\rho \\ -g\rho & 0 & -U(q) & K \\ 0 & -g\rho & K & -U(-q) \end{bmatrix} \quad (11)$$

with $a_{L+} = a_{R+} = \sqrt{\rho}$, $U(\pm q) = -2[\cos(\phi \pm q) - \cos \phi] + K + gn$ and $\mu = -2 \cos \phi - K + gn$. This matrix is diagonalizable and the positive eigenvalues read

$$\varepsilon = \frac{1}{\sqrt{2}} \{ 2K^2 + U(q)^2 + U(-q)^2 - 2g^2n^2 \pm [4K^2U_+^2 + (U_+^2 - 4g^2n^2)U_-^2]^{\frac{1}{2}} \}^{\frac{1}{2}}, \quad (12)$$

where $U_+ = U(q) + U(-q)$ and $U_- = U(q) - U(-q)$.

The excitation spectrums in the Meissner phase under different g and K are shown in Fig. 7. Obviously, the excitation spectrum is symmetry about $q = 0$ and the excitation energy $\varepsilon > 0$. The system is energetic stable in the Meissner phase, which corresponds to the superfluid characteristics of the ground state. Figure 7(a) shows the difference between

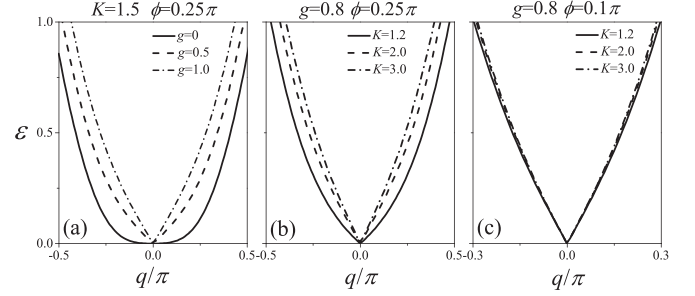


FIG. 7. Excitation spectrum in the Meissner phase for various values of g (a) and K [(b) and (c)].

excitation spectrums with and without atomic interaction. The atomic interaction sharpens the excitation spectrum and provides a single phonon mode close to $q = 0$. In addition, it can be seen from Figs. 7(b) and 7(c) that the excitation spectrum is sharpened with the increase of K and larger ϕ makes the change of excitation spectrum against K more obvious. Furthermore, by comparison, the increase of ϕ makes the excitation spectrum smoother.

B. Excitation spectrum in the BL and vortex phases

In the BL and vortex phases, the ground state with nonzero quasimomentum $k = \pm k_0$ has a twofold degeneracy. The numerical result of Eq. (10) for the excitation spectrums in the BL and vortex phases ($k = \pm k_0$) under different K , g , and ϕ are shown in Fig. 8.

In the BL phase, only one of the two minima is macroscopically populated, so the excitation spectrum ε is obtained with the plane-wave state and is asymmetric about $q = 0$ [Figs. 8(a1)–8(c1)]. The excitation energy $\varepsilon > 0$, the ground state is energetic stable, which corresponds to the stable phase diagram. Furthermore, in addition to phonon mode branches, there is also a rotonlike mode, and g and K enhance the excitation energy of the rotonlike mode and make the rotonlike mode close to phonon mode. When g and K go up to a certain value, the rotonlike mode disappear and the excitation spectrum degenerates to the case of the Meissner phase. The magnetic flux smoothes the excitation spectrum causing the rotonlike mode to move away from phonon mode, thus promoting the generation of vortex phase.

The vortex phase is characterized by a macroscopic occupation of a superposition state involving two momentum modes $k = \pm k_0$, the excitation spectrum ε is obtained with the superposition state. Therefore, different from BL phase, the excitation spectrum in vortex phase is symmetric about $q = 0$ and has two symmetric rotonlike modes [Figs. 8(a2)–8(c2)]. In the vortex phase region, consistent with BL phase, $\varepsilon > 0$ and the ground state is also energetic stable. The excitation energy of the rotonlike mode increases with the increase of g and ϕ , while decreases with the increase of K .

VI. THE NUMERICAL SIMULATION OF THE DYNAMICAL STABILITY

Dynamical instability can cause the system to deviate from its original Bloch state with small instantaneous perturbations,

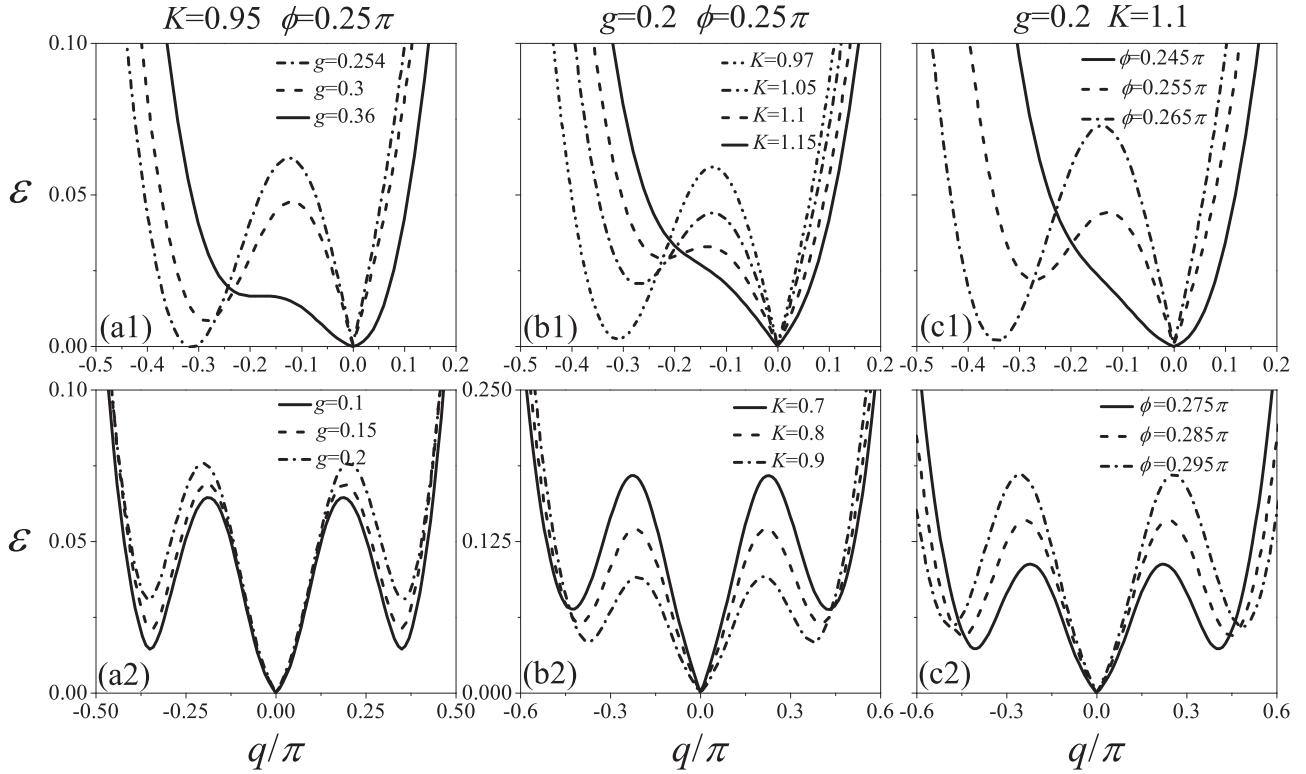


FIG. 8. Excitation spectrums in the BL phase [(a1)–(c1)] and vortex phase [(a2)–(c2)] for various values of g , K , and ϕ .

so it is easy to be simulated numerically. Through the numerical simulation of Eq. (3), the dynamical instability can be verified through the time evolution of the Bloch wave. Figure 9 shows the time evolution diagrams of the Bloch wave in the Meissner phase region as marked by A and B

in Fig. 6(a) and the BL phase region as marked by C and D in Fig. 6(a), respectively. For the zero quasimomentum state, i.e., the ground state is in the Meissner phase, the superfluid always occurs near the center of the Brillouin area ($k = 0$), corresponding to the point A in Fig. 6(a). In this

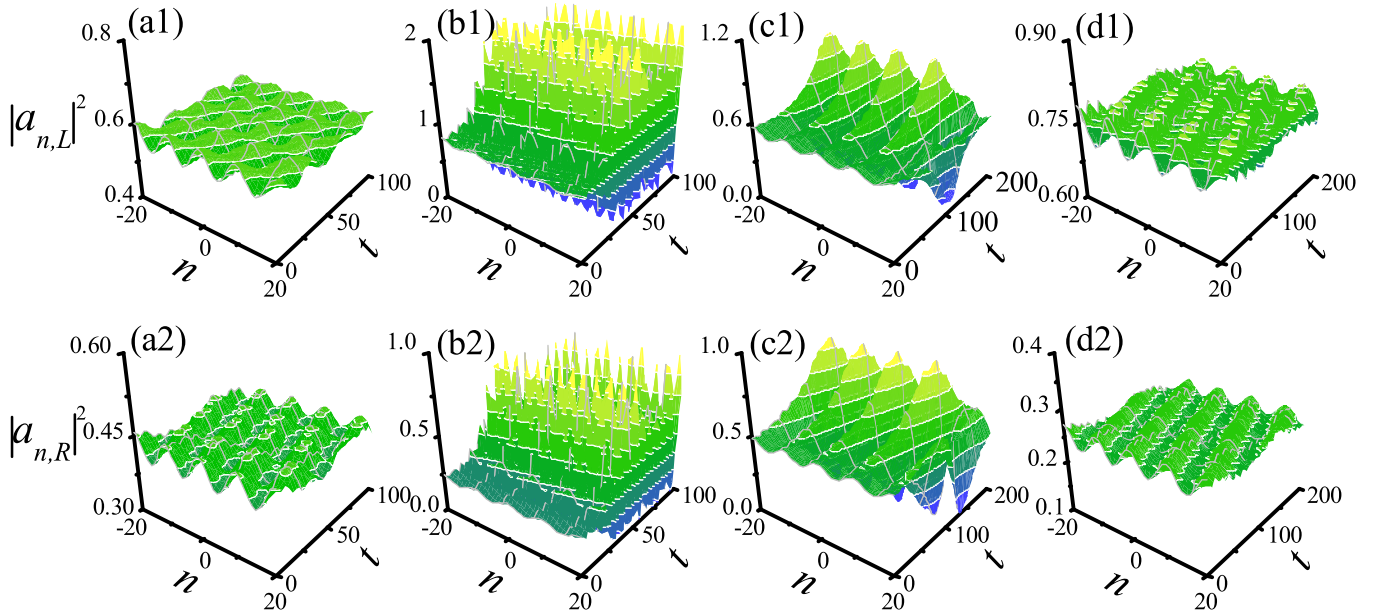


FIG. 9. The time evolution of the Bloch wave in different phase regions as marked by A, B, C, and D in Fig. 6(a). $g = 0.2$, $\phi = \pi/4$, and $q = 0.2\pi$. [(a1) and (a2)] $k = 0.05\pi$ and $K = 1.5$, as marked by A in Fig. 6(a); [(b1) and (b2)] $k = 0.73\pi$ and $K = 1.5$, as marked by B in Fig. 6(a); [(c1) and (c2)] $k = 0.02\pi$ and $K = 1.0$, as marked by C in Fig. 6(a); [(d1) and (d2)] $k = 0.16\pi$ and $K = 1.1$, as marked by D in Fig. 6(a).

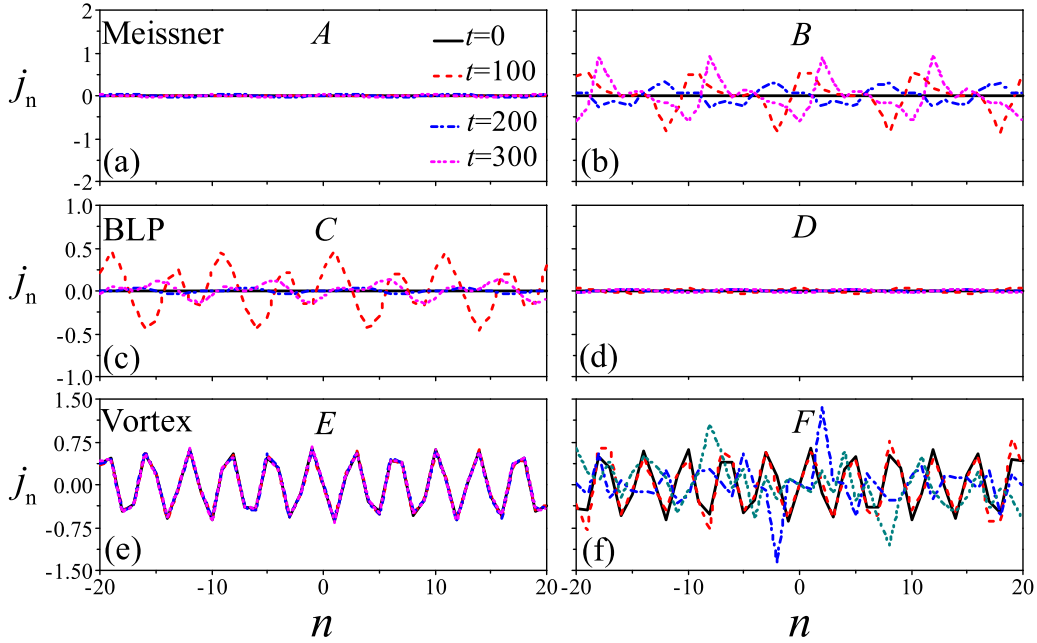


FIG. 10. The exciting rung current j_n in different states as marked by A, B, C, D, E, and F in Fig. 6(a) as a function of lattice site n for different times. $g = 0.2$, $\phi = \pi/4$, and $q = 0.2\pi$. (a) $k = 0.05\pi$ and $K = 1.5$; (b) $k = 0.73\pi$ and $K = 1.5$; (c) $k = 0.02\pi$ and $K = 1.0$; (d) $k = 0.16\pi$ and $K = 1.1$; (e) $k = 0.27\pi$ and $K = 0.75$; and (f) $k = 0.73\pi$ and $K = 0.75$.

region, the ground state is stable and the corresponding Bloch wave periodically oscillates within a certain range due to the perturbation, as shown in Fig. 9(a). When the k is far away from the center of the Brillouin area, the dynamical instability occurs, corresponding to the point B in Fig. 6(a), and the Bloch wave is unstable. As shown in Fig. 9(b), the amplitude of the Bloch wave suddenly increases with time and the whole system is unstable. For the nonzero quasimomentum state, i.e., the ground state is in the BL phase, the dynamical instability occurs near the center of the Brillouin area and the superfluid always occurs near $k = k_0$ area. Figures 9(c) and 9(d) show the numerical simulation of the states as marked by the point C in the dynamical unstable region and the point D in the superfluid region [see Fig. 6(a)], respectively. The numerical results are in good agreement with the theoretical results.

In addition, in order to further explore the superfluidity characteristics, the exciting rung current j_n is numerically simulated. Figure 10 shows j_n in different states as marked by A, B, C, D, E, and F in Fig. 6(a) as a function of lattice site n for different times. Figures 10(a) and 10(b) and Figs. 10(c) and 10(d) show the results with the plane-wave state in the Meissner phase and BL phase, respectively. It can clearly see that in the superfluid region [Figs. 10(a) and 10(d)], corresponding to the points as marked by A and D in Fig. 6(a), when $t = 0$, $j_n = 0$ and when $t > 0$, $j_n \rightarrow 0$. This shows that the particles only propagate on the two legs and do not interfere with each other and the system is stable. However, in the dynamical unstable region [Figs. 10(b) and 10(c)], corresponding to the points as marked by B and C in Fig. 6(a), $j_n \neq 0$ and the perturbation of j_n increases obviously and j_n changes disorderly with time. This indicates that the particles move disorderly in the two-legged ladder and proves that the system is dynamical unstable. In the vortex

phase, the particle number density is modulated between two ladder legs. Figures 10(e) and 10(f) show the results with the superposition state in the vortex phase, corresponding to the points as marked by E and F in Fig. 6(a). In the superfluid region [Fig. 10(e)], j_n oscillates around 0 along the rung and does not change with time, which well capture the propagation characteristics of the particles under the vortex phase. In the dynamical unstable region [Fig. 10(f)], the oscillation of j_n with time becomes disorderly, which indicates that the dynamic instability makes the propagation of the particles become disorderly. This further proves that the dynamical stability of the system can be well revealed by the plane-wave state in the Meissner and BL phases and the superposition state in the vortex phase.

VII. CONCLUSION

In this work, we have investigated the stability and superfluidity of BEC with atomic interaction trapped in two-leg ladder subject to an artificial magnetic field. By studying the dispersion relation, three phases in the ground state are obtained: the Meissner phase, the BL phase, and the vortex phase. The dispersion relation strongly depend on the magnitude of atomic interaction strength, the rung-to-leg coupling ratio and the magnetic flux. The transition of the vortex-BL-Meissner or vortex-Meissner phase is vividly demonstrated by the evolution of the chiral current and the quasimomentum of the ground state. In addition, we discuss the energetic and dynamical stability of the system. The stability phase diagram in the full parameter space is presented, and the dependence of superfluidity on the dispersion relation is illustrated explicitly. The superfluid region closely related to quasimomentum of the ground state, which can be precisely manipulated by the atomic interaction strength, the rung-to-leg coupling ratio

and magnetic flux. Atomic interaction strength can produce dynamical instability in the energetic unstable region and can expand the superfluid region. Furthermore, the excitation spectrums in the three phases are studied, respectively. The excitation spectrums present a phonon mode at long wavelength in the Meissner phase and one or two rotonlike modes in the BL or vortex phase. The energetic stability of the system can be well described by the excitation spectrum. Finally, through the numerical simulation, the dynamical instability of the system is verified by the time evolution of the Bloch wave and the exciting rung current. This provides a possible way to design the superfluid of the system experimentally.

ACKNOWLEDGMENTS

This work is supported by the National Natural Science Foundation of China under Grants No. 11764039, No. 11847304, No. 11865014, No. 11475027, No. 11305132, and No. 11274255; by Natural Science Foundation of Gansu Province under Grants No. 17JR5RA076 and No. 20JR5RA526; by Scientific research project of Gansu higher education under Grant No. 2016A-005; by Innovation capability enhancement project of Gansu higher education under Grants No. 2020A-146 and No. 2019A-014; and by Creation of science and technology of Northwest Normal University under Grant No. NWNLU-LKQN-18-33.

-
- [1] H. Edri, B. Raz, N. Matzliah, N. Davidson, and R. Ozeri, *Phys. Rev. Lett.* **124**, 163401 (2020).
- [2] Y. V. Kartashov and D. A. Zezyulin, *Phys. Rev. Lett.* **122**, 123201 (2019).
- [3] B. A. Malomed, N. N. Rosanov, and S. V. Fedorov, *Phys. Rev. E* **97**, 052204 (2018).
- [4] C. Wang, G. Theocharis, P. G. Kevrekidis, N. Whitaker, K. J. H. Law, D. J. Frantzeskakis, and B. A. Malomed, *Phys. Rev. E* **80**, 046611 (2009).
- [5] E. Kengne and W. M. Liu, *Phys. Rev. E* **98**, 012204 (2018).
- [6] M. Mizoguchi, Y. Zhang, M. Kunimi, A. Tanaka, S. Takeda, N. Takei, V. Bharti, K. Koyasu, T. Kishimoto, D. Jaksch, A. Glaetzle, M. Kiffner, G. Masella, G. Pupillo, M. Weidemüller, and K. Ohmori, *Phys. Rev. Lett.* **124**, 253201 (2020).
- [7] H. Ozawa, S. Taie, T. Ichinose, and Y. Takahashi, *Phys. Rev. Lett.* **118**, 175301 (2017).
- [8] N. Welch, M. T. Greenaway, and T. M. Fromhold, *Phys. Rev. A* **96**, 053623 (2017).
- [9] Lj. Hadžievski, G. Gligorić, A. Maluckov, and B. A. Malomed, *Phys. Rev. A* **82**, 033806 (2010).
- [10] G. Liu, N. Hao, S. L. Zhu, and W. M. Liu, *Phys. Rev. A* **86**, 013639 (2012).
- [11] R. A. Williams, S. Al-Assam, and C. J. Foot, *Phys. Rev. Lett.* **104**, 050404 (2010).
- [12] A. Kato, Y. Nakano, K. Kasamatsu, and T. Matsui, *Phys. Rev. A* **84**, 053623 (2011).
- [13] M. Aidelsburger, M. Atala, M. Lohse, J. T. Barreiro, B. Paredes, and I. Bloch, *Phys. Rev. Lett.* **111**, 185301 (2013).
- [14] H. Miyake, G. A. Siviloglou, C. J. Kennedy, W. C. Burton, and W. Ketterle, *Phys. Rev. Lett.* **111**, 185302 (2013).
- [15] E. Orignac, R. Citro, M. Di Dio, and S. De Palo, *Phys. Rev. B* **96**, 014518 (2017).
- [16] K. Kasamatsu and K. Sakashita, *Phys. Rev. A* **97**, 053622 (2018).
- [17] A. R. Kolovsky, *Europhys. Lett.* **93**, 20003 (2011).
- [18] Y. J. Lin and I. B. Spielman, *J. Phys. B* **49**, 183001 (2016).
- [19] M. Łącki, H. Pichler, A. Sterdyniak, A. Lyras, V. E. Lembessis, O. Al-Dossary, J. C. Budich, and P. Zoller, *Phys. Rev. A* **93**, 013604 (2016).
- [20] R. Bai, S. Bandyopadhyay, S. Pal, K. Suthar, and D. Angom, *Phys. Rev. A* **98**, 023606 (2018).
- [21] S. Pal, R. Bai, S. Bandyopadhyay, K. Suthar, and D. Angom, *Phys. Rev. A* **99**, 053610 (2019).
- [22] R. Sachdeva, M. Singh, and T. Busch, *Phys. Rev. A* **95**, 063601 (2017).
- [23] S. Uchino and A. Tokuno, *Phys. Rev. A* **92**, 013625 (2015).
- [24] S. Greschner and F. Heidrich-Meisner, *Phys. Rev. A* **97**, 033619 (2018).
- [25] R. Sachdeva, F. Metz, M. Singh, T. Mishra, and T. Busch, *Phys. Rev. A* **98**, 063612 (2018).
- [26] Y. Zheng, S. P. Feng, and S. J. Yang, *Phys. Rev. A* **97**, 043627 (2018).
- [27] J. D. Chen, H. H. Tu, Y. H. Wu, and Z. F. Xu, *Phys. Rev. A* **102**, 043322 (2020).
- [28] D. Hügel, H. U. R. Strand, P. Werner, and L. Pollet, *Phys. Rev. B* **96**, 054431 (2017).
- [29] M. Iskin, *Eur. Phys. J. B* **85**, 76 (2012).
- [30] N. Goldman, J. C. Budich, and P. Zoller, *Nat. Phys.* **12**, 639 (2016).
- [31] M. Atala, M. Aidelsburger, M. Lohse, J. T. Barreiro, B. Paredes, and I. Bloch, *Nat. Phys.* **10**, 588 (2014).
- [32] M. Piraud, F. Heidrich-Meisner, I. P. McCulloch, S. Greschner, T. Vekua, and U. Schollwöck, *Phys. Rev. B* **91**, 140406(R) (2015).
- [33] R. Wei and E. J. Mueller, *Phys. Rev. A* **89**, 063617 (2014).
- [34] S. Greschner, M. Piraud, F. Heidrich-Meisner, I. P. McCulloch, U. Schollwöck, and T. Vekua, *Phys. Rev. A* **94**, 063628 (2016).
- [35] N. Victorin, P. Pedri, and A. Minguzzi, *Phys. Rev. A* **101**, 033618 (2020).
- [36] S. S. Natu, *Phys. Rev. A* **92**, 053623 (2015).
- [37] A. Keles and M. Ö. Oktel, *Phys. Rev. A* **91**, 013629 (2015).
- [38] B. Wu and Q. Niu, *New J. Phys.* **5**, 104 (2003).
- [39] C. Raman, M. Köhl, R. Onofrio, D. S. Durfee, C. E. Kulewicz, Z. Hadzibabic, and W. Ketterle, *Phys. Rev. Lett.* **83**, 2502 (1999).
- [40] A. Trombettoni and A. Smerzi, *Phys. Rev. Lett.* **86**, 2353 (2001).
- [41] D. Hügel and B. Paredes, *Phys. Rev. A* **89**, 023619 (2014).